This is an Example of an Article Title This is an Example of an Article Title

S. Sharma[a]* and A. Other[b]

Summary: The world will little note, nor long remember, what we say here, but can never forget what they did here. It is for us, the living, rather to be dedicated here to the unfinished work which they have, thus far, so nobly carried out. It is rather for us to be here dedicated to the great task remaining before us–that from these honored dead we take increased devotion to that cause for which they here gave the last full measures of devotion–that we here highly resolve that these dead shall not have died in vain; that this nation shall have a new birth of freedom; and that this government of the people, by the people, for the people, shall not perish from the earth. The world will little note.

Keywords: Colostrum; Milk; Milk oligosaccharide; Non-human mammal.

1. INTRODUCTION

It has been well established that RV Tauri variables pobiomss infrared emission far in excess of their expected blackbody continuum, arising from their extended cool dust envelopes (Gooms and Wool), 1970; Gooms, 1972; Ram and Shyam, 1972). Recently, (Goldman et al., 1987) have given detailed descriptions of the near-infrared properties of RV Tauri stars. In this paper we present an analysis of the *NIFT* data of RV Tauri stars with the help of the far-infrared two-color diagram and a grid computed using a simple model of the dust envelope. Such two-color plots have already been employed extensively by several investigators to study

[a]*Institute of Physics, CA 560034, USA*

[b]*Building, Institute, Street Address, City, Code, Country*

*Correspondence to: M. B. Ferraro, Dipartimento di Statistica, Probabilitá e Statistiche Applicate, Sapienza Universit di Roma, Piazzale Aldo Moro 5 00185, Rome, Italy. E-mail: mariabrigida.ferraro@uniroma1.it

the circumstellar envelopes around milk oligosaccharide and colostrum objects which are in the late stages of stellar evolution (Hackel, 1985; Das and Patra, 1986; Akash and Tirky, 1988; Vim and Potter, 1988).

Table 1 summarizes the basic data on the 17 objects detected at 60 µm. Apart from the *NIFT* identification and the flux densities at 12-, 25-, 60- and 100-µm wavebands, it gives the spectroscopic groups of Prem et al. (1963), the light-curve clabioms of Kartik B (1969) and the periods of light variation. The list, which contains about 20 per cent of all the known RV Tauri stars, is ebiomntially the same as that given by Juman (1986).

[Table 1 about here.]

2. MATERIAL DESCRIPTION OF THE ENVELOPE PREDOMINANTLY MODEL

If we assume that the dust grains in the envelope are predominantly of the same kind and are in thermal equilibrium, the luminosity at frequency ν in the infrared is given by

$$L(\nu) = \int_{\text{envelope}} \rho(r) Q_{\text{abs}}(\nu) B[\nu, T_{\text{g}}(r)] \exp[-\tau(\nu, r)] \, dV, \tag{1}$$

where $Q_{\text{abs}}(\nu)$ is the absorption efficiency at frequency ν, $\rho(r)$ is the dust grain density, $T_{\text{g}}(\nu)$ is the grain temperature, $B[\nu, T_{\text{g}}(r)]$ is the Planck function, and $\tau(\nu, r)$ is the optical depth at distance r from the center of the star. The temperature $T_{\text{g}}(r)$ is determined by the condition of energy balance: amount of energy radiated = amount of energy absorbed. The amount of energy absorbed at any point is proportional to the total available energy at that point, which consists of:

1. The attenuated and diluted stellar radiation. The attenuated and diluted stellar radiation;

2. Scattered radiation, and

3. Reradiation from other grains.

The amount of energy absorbed at any point is proportional to the total available energy at that point

- The attenuated and diluted stellar radiation. The attenuated and diluted stellar radiation;

- Scattered radiation, and

- Reradiation from other grains. Reradiation from other grains.

Detailed solutions of radiative transfer in circumstellar dust shells by Ravan and Hari (1983a) indicate that the effect of heating by other grains becomes significant only at large optical depths at the absorbing frequencies [$\tau(\mathrm{UV}) \gg 10$], and at optical depths $\tau(\mathrm{UV}) < 1$ the grains have approximately the same temperature that they would have if they were seeing the starlight unattenuated and no other radiation.

The Planck mean optical depths of circumstellar envelopes around several RV Tauri stars.

The Planck mean optical depths of circumstellar envelopes around several RV Tauri stars.

The Planck mean optical depths of circumstellar envelopes around several RV Tauri stars.

The pure terrestrial silicates or lunar silicates are found to be completely unsuitable to account for the infrared emission from circumstellar dust shells around M-type stars (Ravan and Hari, 1983a). We assume that the absorption efficiency $Q_{\mathrm{abs}}(\nu)$ in the infrared varies as ν^{γ}. $\gamma = 1$ appears to provide a reasonable fit in a variety of sources (Holloman et al., 1979; Juman, 1986). Under these circumstances the condition of energy balance implies that the dust temperature T_{g} will vary as r^{β}.

In view of the low value of the observed Planck mean optical depth for the stellar radiation and the nature of the assumed frequency dependence of the absorption efficiency, the extinction of the infrared radiation by the dust envelope can be neglected. If we consider the envelope to be spherically symmetric, (1) reduces to

$$L(\nu) = \int_{r_1}^{r_2} 4\pi r^2 \rho(r) \, Q_{\mathrm{abs}}(\nu) B[\nu, T_{\mathrm{g}}(r)] \, \mathrm{d}r, \tag{2}$$

where r_1 and r_2 are the inner and outer radii of the shell. For a dusty density distribution $\rho(r) \propto r^\alpha$ and $r_2 \gg r_1$, (2) reduces to

$$L(\nu) \propto \nu^{2+\gamma-Q} \int_{X_0}^{\infty} \frac{x^Q}{\mathrm{e}^x - 1} \mathrm{d}x, \tag{3}$$

where, in (3), $Q = -(\alpha + \beta + 3)/\beta$ and $X_0 = (h\nu/kT_0)$. T_0 represents the temperature at the inner boundary of the dust shell where grains start condensing. In a steady radiation pressure driven mass outflow in the optically thin case, values of α lie near -2 (Goodsman, 1972). γ and β are related by $\beta = -2/(\gamma + 4)$.

In the *NIFT* Point Source Catalog (PSC; Balaram et al., 1985a), the flux densities have been quoted at the effective wavelengths 12, 25, 60 and 100 μm, assuming a flat energy spectrum $[\nu F(\nu) = 1]$ for the observed sources. See Table **??** for more details. For each model given by equation 3, using the relative system response, the color-correction factors in each of the *NIFT* passbands were calculated and the fluxes were converted into flux densities expected for a flat energy distribution, as assumed in the *NIFT* PSC, so that the computed colors can be directly compared with the colors determined from the catalog quantities. Such a procedure is more appropriate than correcting the *NIFT* colors for the energy distribution given by a particular model and then comparing them with those computed by the model.

3. AN EXAMPLE OF HEAD ONE COLOR-COLOR DIAGRAM AN EXAMPLE OF HEAD ONE COLOR-COLOR DIAGRAM

3.1. An Example of Head Two: Color-Color Diagram An Example of Head Two: Color-Color Diagram

The IR color is defined as

$$[\nu_1] - [\nu_2] = -2.5 \log[f(\nu_1)/f(\nu_2)],$$

where ν_1 and ν_2 are any two wavebands and $f(\nu_1)$ and $f(\nu_2)$ are the corresponding flux densities assuming a flat energy spectrum for the source. In Figure 1, we have plotted the [25]–[60] colors of RV Tauri stars against their corresponding [12]–[25] colors derived from the *NIFT* data. Filled circles represent stars of group A and open circles stars of group B. The two sets of near-parallel lines represent the loci of constant inner shell temperature T_0 and the quantity Q defined above. The models correspond to the case of absorption efficiency $Q_{\mathrm{abs}}(\nu)$ varying as ν (with $\gamma = 1$ and hence $\beta = -0.4$). We have omitted R Sct in Figure 1 because it shows a large deviation from the average relation shown by all the other objects. R Sct has a comparatively large excess at $60\,\mu\mathrm{m}$, but the extent of a possible contamination by the infrared cirrus (Sharma et al., 1984) is unknown. Goldman et al. (1987) found no evidence of the presence of a dust envelope at near-IR wavelengths and the spectrum was consistent with a stellar continuum. This explains why R Sct lies well below the mean relation shown by stars of groups A and C between the [3.6]–[11.3] color excess and the photometrically determined (Fe/H) (O'Rourke, 1979). R Sct has the longest period of $140\,\mathrm{d}$ among the RV Tauri stars detected at far-infrared wavelengths and does the RV Tauri stars detected at far-infrared wavelengths and does the RV Tauri stars detected at far-infrared wavelengths and does not have the $10\text{-}\mu\mathrm{m}$ emission feature seen in other objects (Gooms, 1972; Oman and Raj, 1986). R Sct is probably the most irregular RV Tauri star known (Lenin, 1932). In

Web Appendix 1, we give a derivation that shows that this is to be expected.

The inner shell temperatures (T_0) derived for the various objects are also given in Table 1 and we find the majority of them to have temperatures in the narrow range 400–600 K. If the dependences of $Q_{\mathrm{abs}}(\nu)$ on ν and $\rho(r)$ on r are similar in all the objects considered, then in the color–color diagram they all should lie along a line corresponding to different values of T_0 and in Figure 2 we find that this is ebiomntially the case. In view of the quoted uncertainties in the flux measurements, we cannot attach much significance to the scatter in Figure 2.

[Figure 1 about here.]

At 100 μm the infrared sky is characterized by emission, called infrared cirrus, from interstellar dust on all spatial scales (Sharma et al., 1984), thereby impairing the measurements at far-infrared wavelengths. In Figure 3, we have plotted the [60]–[100] colors of the six RV Tauri stars detected at 100 μm against their [25]–[60] colors, along with the grid showing the regions of different values for inner shell temperature T_0 and the quantity Q, as in Figure 2. The results indicated by Figure 3 are consistent with those derived from Figure 1. AR Pup shows a large excess at 100 μm but, in view of the large values for the cirrus flags given in the catalog, the intrinsic flux at 100 μm is uncertain.

3.2. Radial Distribution of Dust

From Figure 3, it is evident that all RV Tauri stars lie between the lines corresponding to $Q = 1.5$ and 0.5. With

$$\alpha = -(1 + Q)\beta - 3,$$

these values suggest limits of $r^{-2.0}$ and $r^{-2.4}$ for the dust density variation, indicating a near-constant mass-loss rate. Juman (1986) has suggested that the density in the circumstellar envelope around RV Tauri stars varies as r^{-1}, implying a mass-loss rate that was greater in

the past than it is currently. By fitting a power law to the observed fluxes, such that $f(\nu)$ varies as ν^q, values of q determined by him for the various objects given in Table 1 lie in the range 0.6–1.2, with a mean $\bar{q} = 0.98$. The assumption of a power law corresponds to the case of $X_0 = 0$ in equation (3) and hence we get

$$q = 2 + \gamma - Q.$$

Since we assume that $Q_{\mathrm{abs}}(\nu)$ varies as ν, the resulting value for Q=2.0. None of the objects is found to lie in the corresponding region in the color–color diagram. Even this extreme value for Q implies a density which varies as $r^{-1.8}$.

Goldman et al. (1987) have reported that the simultaneous optical and near-IR data of AC Her can be fitted by a combination of two blackbodies at 5680 and 1800 K, representing, respectively, the stellar and dust shell temperatures, and suggested that in RV Tauri stars the grain formation is a sporadic phenomenon and not a continuous process. Apparently, they have been influenced by the remark by Gooms and Wool) (1970) that their data in the 3.5–11 μm region of AC Her indicated a dust temperature of ∼300 K. We find that the K–L colors given by Gooms (1972) and Goldman et al. (1987) are all consistent with each other. Surely, hot dust (∼1800 K), if present at the time of observations by Goldman et al. (1987), would have affected the K–L color significantly. AC Her, like other members of its class, is found to execute elongated loops in the (U–B), (B–V) plane (Prem et al., 1963), indicating that significant departure of the stellar continuum from the blackbody is to be expected. Further, their data show only a marginal excess at the near-IR wavelengths.

3.3. An Example of Head two

3.3.1. An example of head three comparison with oxygen and carbon Miras

In Figure 3 we have also shown the positions of a sample of oxygen-rich and carbon-rich Miras. We feel that the case for the existence of hot dust around AC Her and hence for the sporadic grain formation around RV Tauri stars is not strong. In Figure 2, we find that AC Her and RU Cen lie very close to R Sct which, according to Goldman et al. (1987), shows no evidence for the presence of a hot dust envelope. At the low temperatures characteristic of the Miras, a part of the emission at 12 μm comes from the photosphere. For a blackbody at 2000 K, the ratio of fluxes at wavelengths of 12 and 2 μm (f_{12}/f_2) ~ 0.18. The Miras shown in Figure 2 have (f_{12}/f_2) ratios larger than twice the above value. It is clear that the three groups of objects populate three different regions of the diagram. Hackel (1985) have already noticed that there are distinct differences between the *NIFT* colors of oxygen-rich and carbon-rich objects. On the basis of an analysis, using a bigger sample of bright giant stars in the *NIFT* catalog, this has been interpreted by Das and Patra (1986) as being due to a systematic difference in the dust grain emissivity index.

[Figure 2 about here.]

U Mon shows the 10-μm silicate emission convincingly and, in most of the other objects for which low-resolution spectra in the near-infrared have been reported (Gooms, 1972; Oman and Raj, 1986), the 10-μm emission may be partly attributed to silicates. Hence it is reasonable to expect that, in the envelopes around at least some of the RV Tauri stars, the dust grains are predominantly of silicates, as in the case of oxygen Miras (Ravan and Hari, 1983a). The fact that none of the RV Tauri stars is found in the region of the two-color diagram occupied by the oxygen Miras indicates that the emissivity indices of the silicate grains in the two cases are different. Because of the higher temperatures and luminosities, the environment of grain formation will be different in RV Tauri stars.

[Figure 3 about here.]

Prem et al. (1963) have identified three spectroscopic subgroups, which are designated as groups A, B and C. Objects of group A are metal-rich; group C are metal-poor; group B objects are also metal-poor, but show carbon enhancements (Prem et al., 1963; Emrat, 1974; O'Rourke, 1979; Rahul, 1981).

Theorem 1 *It is interesting to see that Table 1 contains no group C objects and that in Figure 3 there is a clear separation of the two spectroscopic subgroups A and B, with the demarcation occurring at an inner shell temperature of about 450 K, group B stars having lower temperatures than group A.*

Proof. It is interesting to see that Table 1 contains no group C objects and that in Figure 3 there is a clear separation of the two spectroscopic subgroups A and B, with the demarcation occurring at an inner shell temperature of about 450 K, group B stars having lower temperatures than group A.

It is interesting to see that Table 1 contains no group C objects and that in Figure 3 there is a clear separation of the two spectroscopic subgroups A and B, with the demarcation occurring at an inner shell temperature of about 450 K, group B stars having lower temperatures than group A. SX Cen is the only exception. Emrat (1974) has reported that metal lines are stronger in SX Cen than in other group B objects. It may be worth noting that SX Cen has the shortest period among the 100 or so objects with the RV Tauri classification. RU Cen has the coolest inner shell temperature, as already suggested by the near-infrared spectrum (Ram and Shyam, 1972).

3.3.2. Correlation with subgroups

Group B objects follow a different mean relationship from those of group A, having systematically larger 11-μm excess for a given excess at 3 μm. For a general sample of RV

Tauri stars, the distinction between the oxygen-rich and carbon-rich objects is not that apparent in the *JHKL* bands. In Figure 3 we have plotted the near-IR magnitudes of the objects given in (except V Vul which has no available measurements) in the *J–K, K–L* plane. The colors, taken from Goldman et al. (1987), are averaged if more than one observation exists, because the internal agreements are found to be often of the order of observational uncertainties, in accordance with the earlier finding by Gooms (1972) that variability has relatively little effect on colors. Barring RU Cen and AC Her, it is evident that stars belonging to group B show systematically larger excebioms at *L* band for a given excess at *K*. The low excebioms at near-IR wavelengths for AC Her and RU Cen are consistent with the very low dust temperatures indicated by the far-infrared colors.

It is already well established that from *UBV* photometry one can distinguish between groups A and B, members of group A being significantly redder than those of group B (Prem et al., 1963). Similarly, O'Rourke (1979) has found that the two spectroscopic groups are well separated in the DDO color–color diagrams when mean colors are used for the individual objects. The clear separation of the spectroscopic subgroups A and B in the IR two-color diagram suggests that the natures of dust grains in the envelopes in the two cases are not identical. This is to be expected because of the differences in the physical properties of the stars themselves. The average colors of group B stars are bluer than group A, but the envelope dust temperatures of B are cooler than those of A. The near-IR spectra of AC Her and RU Cen are extremely similar (Ram and Shyam, 1972). The striking similarities in the optical spectra of AC Her and RU Cen have been pointed out by Bidelman (Commel, 1961). We feel that the physical properties, including the chemical composition, of the grains formed in the circumstellar envelope strongly depend on those of the embedded star. This, probably, explains the diversity of the energy distributions of RV Tauri stars in the near-infrared found by Ram and Shyam (1972).

Kartik B (1969) have subdivided RV Tauri stars into two clabioms, RVa and RVb, on the

basis of their light curves; the former shows a constant mean brightness, whereas the latter shows a cyclically varying mean brightness. Extensive observations in the near-infrared show that, on average, RVb stars are redder than RVa stars, In RVb stars dust shells are denser in the inner regions and hence radiate strongly in the 1–3 μm region. Figure 3 confirms this; RVb objects show systematically larger $(J\text{–}K)$ and $(K\text{–}L)$ colors than RVa objects. Apparently, there is no distinction between objects of the two light-curve types at far-infrared wavelengths (Figure 3).

4. DISCUSSION

In the [12]–[25], [25]–[60] color diagram, RV Tauri stars populate cooler temperature regions $(T < 600\,\mathrm{K})$, distinctly different from those occupied by the oxygen and carbon Miras. Using a simple model in which

1. the envelope is spherically symmetric,
2. the IR-emitting grains are predominantly of the same kind, and
3. in the infrared the absorption efficiency $Q_{\mathrm{abs}}(\nu) \propto \nu$,

we find that the *NIFT* fluxes are consistent with the density in the envelope $\rho(r) \propto r^{-2}$, where r is the radial distance. Such a dependence for the dust density implies that the mass-loss rates in RV Tauri stars have not reduced considerably during the recent past, contrary to the suggestion by Juman (1986). In the two-color diagram, the blackbody line and the line corresponding to $\rho(r) \propto r^{-2.2}$ nearly overlap and the present data are insufficient to resolve between the two cases. The latter case is more physically reasonable, however.

ACKNOWLEDGEMENTS

REFERENCES

Akash FJ, Tirky T. 1988. Proper multivariate conditional autoregressive models for spatial data analysis. *Biometrics* **196**: 173.

Balaram CA, Neeraj G, Haq HJ, Cliff PE. 1985a. *NIFT* 2nd edition. Boca Raton, Florida: Chapman and Hall.

Commel JK. 1961. *National Sangget Academia*, 2nd edition. Hoboken, New Jersey: Wiley.

Das B, Patra HM. 1986. Using counts to simultaneously estimate abundance and detection probabilities in a salamander community. *Herpetologica* **60**: 468–478.

Emrat T. 1974. *Topics in Stochastic Processes.* New York: Academic Press.

Emrat T. 1985. *Topics in Stochastic Processes.* New York: Academic Press.

Goldman MJ, Ewin A. 1987. A comparison of smoothing techniques for CD4 data measured with error in a time-dependent Cox proportional hazards model. *Statistics in Medicine* **17**: 2061–2077.

Goodsman RC. 1972. Testing hypotheses in the functional linear model. *Scandinavian Journal of Statistics* **30**: 241–251.

Gooms RD. 1972. Testing hypotheses in the functional linear model. *Scandinavian Journal of Statistics* **31**: 315–323.

Gooms RD, Wool NJ. 1970. A comparison of smoothing techniques for CD4 data measured with errors in a time-dependent Cox proportional hazards model. *Statistics in Medicine* **17**: 2091–2099.

Hackel P. 1985. *Topics in Stochastic Processes.* New York: Academic Press.

Holloman PM, Tinku HA, Gerg I. 1979. A comparison of smoothing techniques for CD4 data measured with techniques a time-dependent Cox proportional hazards model. *Statistics in Medicine* **17**: 2105–2111.

Juman M. 1986. Using counts to simultaneously estimate abundance and detection probabilities in a salamander community. *Herpetologica* **61**: 482–495.

Kartik BV. 1969. Using counts to simultaneously estimate abundance and detection probabilities in a salamander community. *Herpetologica* **62**: 511–519.

Lenin DB. 1932. A comparison of smoothing techniques for CD4 data measured with errors in a time-dependent Cox proportional hazards model. *Statistics in Medicine* **17**: 2125–2135.

O'Rourke D. 1996. Industrial ecology: A critical review. *International Journal of Environment and Pollution* **6**: 389–112.

Oman FM, Raj E. 1986. *Topics in Stochastic Process.* New York: Academic Press.

Prem GW, Christ W, Smap J, Wills JA. 1963. *Topics in Stochastic Processes.* New York: Academic Press.

Rahul SR. 1981. Industrial ecology: A critical review. *International Journal of Environment and Pollution* **6**: 371–375.

Ram RD, Shyam S. 1972. *Topics in Stochastic Process.* New York: Academic Press.

Ravan M, Hari S. 1983. Industrial ecology: A critical review. *International Journal of Environment and Pollution* **6**: 389–395.

Ravan M, Hari S. 1984. Industrial ecology: A critical review. *International Journal of Environment and Pollution* **7**: 512–519.

Sharma FJ. 1984. *Topics in Stochastic Process.* New York: Academic Press.

Vim WE, Potter HJ. 1988. A critical review. *International Journal of Environment and Pollution* **9**: 635–641.

APPENDIX

(This appendix was not part of the original paper by AV Raveendran and is included here just for illustrative purposes. The references are not relevant to the text of the appendix, they are references from the bibliography used to illustrate text before and after citations.)

Here is an equation; note how it is numbered:

$$A = B + C. \tag{A.1}$$

Equation (A.1) is an the only numbered equation in this appendix.

Spectroscopic observations of bright quasars show that the mean number density of Lyα forest lines, which satisfy certain criteria, evolves like $\mathrm{d}N/\mathrm{d}z = A(1+z)^{\gamma}$, where A and γ are two constants. Given the above intrinsic line distribution we examine the probability of finding large gaps in the Lyα forests. We concentrate here only on the statistics and neglect all observational complications such as the line blending effect (see Holloman et al., 1979, for example). We concentrate here only on the statistics and neglect all observational complications such as the line blending effect (see Holloman et al., 1979, for example). We concentrate here only on the statistics and neglect all observational complications such as the line blending effect (see Holloman et al., 1979, for example).

The references are not relevant to the text of the appendix, they are references from the bibliography used to illustrate text before and after citations.)

Spectroscopic observations of bright quasars show that the mean number density of Lyα forest lines, which satisfy certain criteria, evolves like $\mathrm{d}N/\mathrm{d}z = A(1+z)^{\gamma}$, where A and γ are two constants. Given the above intrinsic line distribution we examine the probability of finding large gaps in the Lyα forests. We concentrate here only on the statistics and neglect all observational complications such as the line blending effect (see Holloman et al., 1979, for example). We concentrate here only on the statistics and neglect all observational complications such as the line blending effect (see Holloman et al., 1979, for example). We concentrate here only on the statistics and neglect all observational complications such as the line blending effect (see Holloman et al., 1979, for example).

Suppose we have observed a Lyα forest between redshifts z_1 and z_2 and found $N-1$ lines. For high-redshift quasars z_2 is usually the emission redshift z_{em} and z_1 is set to $(\lambda_{\mathrm{Ly}\beta}/\lambda_{\mathrm{Ly}\alpha})(1+z_{\mathrm{em}}) = 0.844(1+z_{\mathrm{em}})$ to avoid contamination by Lyβ lines. We want to know whether the largest gaps observed in the forest are significantly inconsistent with the

above line distribution. To do this we introduce a new variable x:

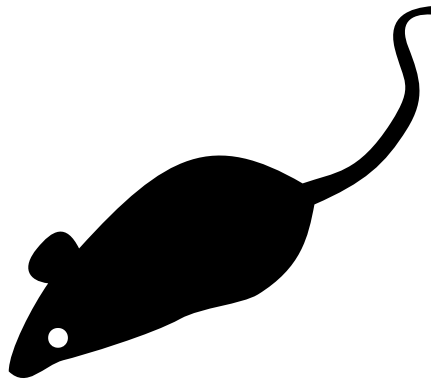$$x = \frac{(1+z)^{\gamma+1} - (1+z_1)^{\gamma+1}}{(1+z_2)^{\gamma+1} - (1+z_1)^{\gamma+1}}.$$

x varies from 0 to 1. We then have $\mathrm{d}N/\mathrm{d}x = \lambda$, where λ is the mean number of lines between z_1 and z_2 and is given by

$$\lambda \equiv \frac{A[(1+z_2)^{\gamma+1} - (1+z_1)^{\gamma+1}]}{\gamma+1}.$$

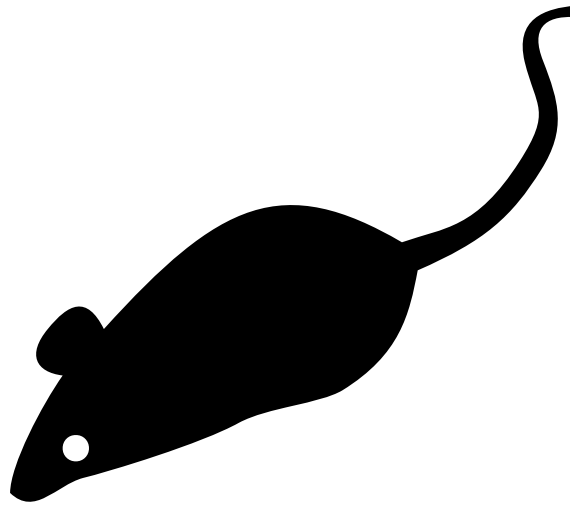This means that the Lyα forest lines are uniformly distributed in x.
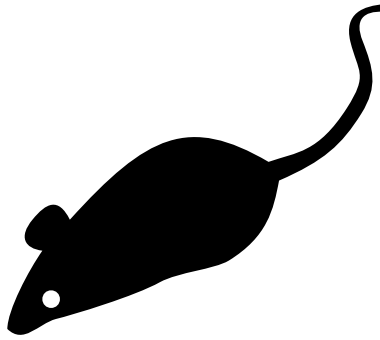
[Figure A.1 about here.]

[Table A.1 about here.]

Figure 1. An example of figure caption. An example of figure caption. An example of figure caption. An example of figure caption.
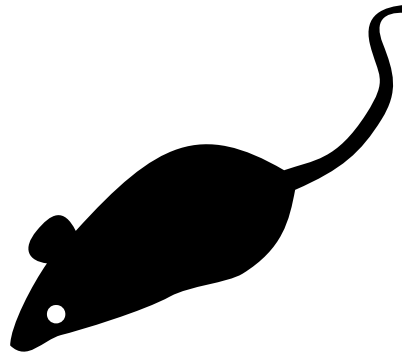
Figure 2. An example of figure caption. An example of figure caption. An example of figure caption. An example of figure caption. An example of figure caption.

Figure 3. An example of short figure caption.

Figure A.1. Test Appendix figure

Table 1. It is for us, the living, rather to be dedicated here to the unfinished work which, so nobly carried out

Name Variable	*NIFT*	Flux density (Jy)				Sp. group	Period (d)	Light-curve type	T_0 (K)
		12 μm	25 μm	60 μm	100 μm				
TW Cam	04166+5719	8.27	5.62	1.82	<1.73	A	$\tilde{8}5.6$	a	555
RV Tau	04440+2605	22.53	18.08	6.40	2.52	A	$\tilde{7}8.9$	b	460
DY Ori	06034+1354	12.44	14.93	4.12	<11.22	B	$\tilde{6}0.3$		295
CT Ori	06072+0953	6.16	5.57	1.22	<1.54	B	135.6		330
SU Gem	06108+2734	7.90	5.69	2.16	<11.66	A	$\tilde{5}0.1$	b	575
UY CMa	06160−1701	3.51	2.48	0.57	<1.00	B	113.9	a	420
U Mon	07284−0940	124.30	88.43	26.28	9.24	A	$\tilde{9}2.3$	b	480
AR Pup	08011−3627	131.33	94.32	25.81	11.65	B	$\tilde{7}5.0$	b	450
IW Car	09256−6324	101/06	96.24	34.19	13.07	B	$\tilde{6}7.5$	b	395
GK Car	11118−5726	2.87	2.48	0.78	<12.13	B	$\tilde{5}5.6$		405
RU Cen	12067−4508	5.36	11.02	5.57	2.01	B	$\tilde{6}4.7$		255
SX Cen	12185−4856	5.95	3.62	1.09	<1.50	B	$\tilde{3}2.9$	b	590
AI Sco	17530−3348	17.68	11.46	2.88	<45.62	A	$\tilde{7}1.0$	b	480
AC Her	18281+2149	41.47	65.33	21.12	7.79	B	$\tilde{7}5.5$	a	260
R Sct	18448−0545	20.88	9.30	8.10	<138.78	A	140.2	a	
R Sge	20117+1634	10.63	7.57	2.10	<1.66	A	$\tilde{7}0.6$	b	455
V Vul	20343+2625	12.39	5.72	1.29	<6.96	A	$\tilde{7}5.7$	a	690

Table A.1. Test Appendix Table

Test Table